RSC Advances

ROYAL SOCIETY OF CHEMISTRY

www.rsc.org/advances

Journal Name

RSCPublishing

ARTICLE

Promoting desulfurization capacity and separation efficiency simultaneously by the novel magnetic Fe_3O_4@PAA@MOF-199

Cite this: DOI: 10.1039/x0xx00000x

Received 00th January 2012,
Accepted 00th January 2012

DOI: 10.1039/x0xx00000x

www.rsc.org/

Tian Jin,[a] Qiang Yang,[a] Chun Meng,[a] Jian Xu,[b] Honglai Liu,[a] Jun Hu*[a] and Hao Ling*[a]

The world becomes more stringent on keep lowering the sulfur concentrations in fuels. To fulfill this expectation, a new type of magnetic desulfurization adsorbent of Fe_3O_4@PAA@MOF-199 was designed and fabricated by a facile two-step assembly approach, in which PAA inventively acted like a bridge to incorporate different amounts of the magnetite Fe_3O_4 into MOF-199 crystal matrix. Fe_3O_4@PAA@MOF-199s were demonstrated to be efficient adsorbents for the removal of S-compounds of thiophene, benzothiophene (BT) and dibenzothiophene (DBT) from a model fuel, and the sulfur saturated adsorption capacity followed the order of DBT > BT > thiophene. The magnetization of Fe_3O_4@PAA@MOF-199s insured the adsorbents a good performance in magnetic separation. The relative high adsorption capacity, the separation efficiency, as well as the stable recyclability indicated that magnetic Fe_3O_4@PAA@MOF-199 would be a promising adsorbent in adsorptive desulfurization.

Introduction

Worldwide environmental legislation becomes more stringent on SOx exhaust levels. It is very important to keep lowering the sulfur concentrations in fuels to 10 ppmw S (parts per million by weight of sulfur) or less.[1-4] Currently, the main industrial process is hydrodesulfurization (HDS) in which sulfur compounds such as thiophene, benzothiophene (BT), and dibenzothiophene (DBT) in fuel feeds, are hydrogenated to hydrocarbons and H_2S. However, this conventional process is not completive for ultra-deep desulfurization because of highly demanded operation conditions and cost, such as high temperature and pressure, extra consumption of H_2, and serious deactivation of catalysts. In addition, refractory aromatic sulfur compounds, especially those with the steric hindrance like DBT and 4,6-dimethyldibenzothiophene (4,6-DMDBT), are inefficient to remove by HDS because of their low reactivity in a low concentration.[5]

Compared with HDS technology, a promising way to remove S-compounds would be adsorption because it can be carried out under ambient temperature and pressure. More importantly, it has the capability to reduce sulfur content to less than 1 ppmw S.[6] Various adsorbents including zeolites[7-9], activated carbons[10-12] have been explored over years. Generally, efficient desulfurization by adsorption comes from the strong interaction between S-compounds and the adsorbent. It has been proposed that incorporating the transition metal ions, such as Cu^+ and Ag^+ into the microporous materials could result in high S-adsorption capacity and high selective desulfurization, which are attributed to the formation of π-complexation between S-compounds and metal ions, as well as direct sulfur−metal (S-M) interaction.[13,14]

Metal-organic frameworks (MOFs) are a promising type of adsorbent because of their highly ordered three-dimensional porous networks, high inner surface areas and large pore volumes. The desulfurization capacity of MOFs was found to be determined by the pore size and shape.[15,16] Li et al.[17] investigated four types of MOFs, and found the adsorption capacity for DBT follows the order of Cu-BTC > Cr-BDC > Cr-BTC >> Cu-BDC, which was considered as a result of the comprehensive effects, not only the suitable pore size and shape, but also the framework structure and exposed Lewis acid site. Jhung et al.[18] embedded $CuCl_2$ into porous MIL-47 (vanadium-benzenedicarboxylate) and achieved a remarkably high saturation adsorption capacity (310 mg BT•g^{-1} at 25 °C). Among numerous MOFs reported so far, one of the most popular adsorbent is the porous copper-benzenetricarboxylate (Cu-BTC, i.e. MOF-199, HKUST-1 or C300), which has been

realized the mass production.[19] Herein, we proposed the use of MOF-199 for the selective adsorption of S-compounds.

For the technique of the desulfurization process, magnetic separation of adsorbents from the fuel based on the superparamagnetic particles is obviously much more convenient and efficient. In fact, magnetic separations have been used in diverse areas,[20-25] which provide a good base for us to design magnetic MOF nanocomposites. Very recently, magnetic MOF/Fe_3O_4 nanohybrides have been successfully fabricated through layer by layer (LBL) method.[26] However, the complicated operation procedure, high solvent consumption, and low coating thickness made it hardly to be a real application. Kaskel et al. prepared superparamagnetic functionalized MOFs by integrating superparamagnetic iron-oxide nanoparticles into polycrystalline MOF aggregates.[27] Although the concept allows the external manipulation of highly microporous MOFs for efficient catalyst separation, the obtained composite material was heterogeneous and hence decreased the separation efficiency.

In the present study, a novel facile synthesis method of magnetic Fe_3O_4@PAA@MOF-199 was proposed. Polyacrylic acid (PAA) chains in this composite acted like a bridge, connecting the inside magnetite nanoparticles Fe_3O_4 and outside MOF-199 layer. The carboxyl group in PAA chain can strongly coordinate with ferric ions as a binding to produce a highly uniform of magnetite submicrospheres on one hand; and can simultaneously coordinate with copper ions as a substrate for the further growth of MOF-199 on the other hand. The desulfurization performances of the magnetic adsorbent were tested for removing thiophene, BT and DBT in n-Octane solvent. The efficiency of magnetic separation and the recycling desulfurization performance were investigated as well.

Experimental section

Chemicals

Analytical grade reagents of ferric chloride ($FeCl_3 \cdot 6H_2O$, ⩾ 99.0%), sodium acetate (NaAc, ⩾99.0%), ethylene glycol (EG, ⩾ 99.0%), copper nitrate ($Cu(NO_3)_2 \cdot 3H_2O$, ⩾ 99.0%), n-Octane (⩾95.0%) were purchased from Sinopharm Chemical Reagent Co., Ltd. Polyacrylic acid (PAA, Mw ≈ 3000), p-xylene (⩾99.0%), and thiophene (99%) were purchased from Aladdin Chemistry Co.. 1,3,5-Benzenetricarboxylic acid (H_3BTC, ⩾ 95%), benzothiophene (⩾ 98%) and dibenzothiophene (⩾ 98%) were purchased from Sigma-Aldrich Co.. All chemicals were used as purchased without further purification.

Synthesis

A two-step assembly approach was adopted for synthesis of Fe_3O_4@PAA@MOF-199. As shown in Scheme 1, the first step is the assembly of $FeCl_3$ and PAA chain, then, the second step is the assembly of Fe_3O_4@PAA submicrospheres and MOF precursors.

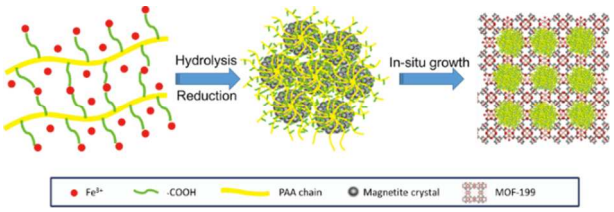

Scheme 1 Possible formation approach of the magnetic Fe_3O_4@PAA@MOF-199 microspheres.

During the first assembly processes, Fe^{3+} ions were firstly coordinated with carboxyl groups on PAA chains, and then were hydrolyzed to $Fe(OH)_3$ by alkali NaAc, and also partially reduced to $Fe(OH)_2$ by ethylene glycol. $Fe(OH)_3$ and $Fe(OH)_2$ were further dehydrated and formed magnetite Fe_3O_4 when heating at 200 °C. For the details, Fe_3O_4@PAA was synthesized using a modified procedure reported by Liang et al.[28] Typically, 1.47 g $FeCl_3 \cdot 6H_2O$ was first completely dissolved in 80 mL ethylene glycol. When 1.04 g PAA was added, the golden yellow aqueous solution was obtained. After stirring for 30 min, 5.40 g NaAc was added into the solution. Following an ultrasonic mixing for 30 min, the whole reaction solution was put into a 100 mL teflon-lined stainless-steel autoclave and heated at 200 °C for 24 h. The synthesized magnetite submicrospheres were washed with ethanol and deionized water for three times and separated by the magnet, respectively. The final product was dispersed and stored in 80 mL ethanol.

During the second assembly processes, Cu^{2+} ions were coordinated with carboxyl groups of PAA chains on the surface of Fe_3O_4@PAA submicrospheres, and then, the unsaturated Cu^{2+} ions were further coordinated with carboxyl groups of H_3BTC for the growth of the first seed layer of MOF-199 crystals. Following that, the MOF-199 crystals would grow up around Fe_3O_4@PAA submicrospheres. Meanwhile, instead of growing around the Fe_3O_4@PAA submicrospheres, MOF-199 crystals may also produce in the bulk solution. For the synthesis details, 1 g $Cu(NO_3)_2 \cdot 3H_2O$ and 0.5 g H_3BTC were completely dissolved in 60 mL EtOH. Then, 5 mL or 15 mL as-synthesized Fe_3O_4@PAA ethanol solution was added into the MOF-199 precursor solution, respectively. After stirring at 80 °C for 2 h, the products of Fe_3O_4@PAA@MOF-199 (L, low Fe_3O_4 content) or Fe_3O_4@PAA@MOF-199 (H, high Fe_3O_4 content) was finally obtained after washing with EtOH, separating through the magnet, and drying at 100 °C. Pure MOF-199 without adding Fe_3O_4@PAA was also synthesized in similar way for comparison.

Characterization

The morphology of samples was characterized by using a Nova NanoS 450 field emission scanning electron microscope (FESEM) operated at 5 kV. All transmission electron microscope images were obtained by using a JEOL JEM-2100 instrument. Powder X-ray diffraction (PXRD) data were collected on a D/Max2550 VB/PC diffractometer (40 kV, 200 mA) using a Cu Kα as the radiation. N_2 adsorption–desorption

isotherms at 77 K were measured by volumetric adsorption analyzer ASAP 2020. The specific surface area was calculated by Brunauer–Emmett–Teller (BET) method. The FTIR spectra were carried out on a Nicolet iS10 FTIR spectrometer with KBr pellet technique. The thermal stability was detected by using a TGA unit (NETZSCH STA 499 F3). About 10 mg of the sample was heated from 25 ^{o}C to 600 ^{o}C at the heating rate of 10 ^{o}C min^{-1} in nitrogen with a flow rate of 40 mL min^{-1}. X-ray photoelectron spectroscopy (XPS) measurement was conducted with a PHI 5000C ESCA spectrometer (Perkin-Elmer, USA) with an Al Kα radiation as the X-ray source. Magnetization of the samples were carried out on a Lakeshore 7407 vibration sample magnetometer (VSM). The inductively coupled plasma atomic emission spectrometry (ICP-AES, Vanan 710) was employed to determine Copper (II) content in samples, and the samples were treated by the mixture of HCl and HNO_3 before the measurement.

Desulfurization measurements

The desulfurization performance of Fe_3O_4@PAA@MOF-199s was tested by the adsorption capacity of sulfur in the model oil, which was prepared by dissolving thiophene, BT or DBT in n-Octane. With a ratio of (0.02 g adsorbent) / (5 mL oil), all adsorption experiments were conducted in a 10 mL glass bottle at 25 ^{o}C under stirring. Prior to adsorption, each adsorbent was vacuumed at 150 ^{o}C for 2 h. The concentration of sulfur in oil was determined by a gas chromatography-flame photometric detector (GC-FPD, GC-950, Haixin Chromatography), which was equipped with a HP-5 capillary column (15 m × 0.53 mm × 1.5 μm film thickness). The adsorption capacity was calculated by

$$Q_i = \frac{W}{M}(C_0 - C_i)\times 10^{-3} \quad (1)$$

Where Q_i is the adsorption capacity of sulfur adsorbed on the adsorbent (mg S•g^{-1} adsorbent), W is the mass of model oil (g), M is the mass of the adsorbent used (g), and C_0 and C_i are the initial and final concentrations of sulfur in the model oil (mg•g^{-1}), respectively.

The saturated adsorption capacity was calculated using the Langmuir adsorption model when the adsorption equilibrium was reached. The adsorption isotherms of Fe_3O_4@PAA@MOF-199s can be plotted according to the Langmuir equation of Eq. 2

$$\frac{C_e}{Q_e} = \frac{C_e}{Q_0} + \frac{1}{Q_0 b} \quad (2)$$

Where C_e is the equilibrium concentration of S-compound (mg•L^{-1}), Q_e is the amount of sulfur adsorbed at equilibrium (mg S•g^{-1}), Q_0 is the saturated adsorption capacity (mg S•g^{-1}), b is the Langmuir constant (L•mg^{-1}). Therefore, the maximum adsorption capacity Q_0, can be obtained from the reciprocal of the slope of the plot of C_e / Q_e against C_e.

Recyclability and regeneration

The separation performance of the adsorbent was determined on a scattering turbidimeter (WGZ-800, Shanke instrument) by measuring the turbidity of the oil after the adsorbent was separated by the magnet. The turbidity of the oil with pure MOF-199 was also determined in the similar way for comparison.

The regeneration of the adsorbent was performed by the solvent extraction. After adsorption and magnetic separation, the adsorbent was extracted by p-xylene for 3 times to remove adsorbed S-compounds and then was dried at 150 ^{o}C overnight. The recycling desulfurization performance was tested by taking the regenerated adsorbent as a fresh adsorbent. The recycling desulfurization was repeated for 5 times.

Results and discussion

Characterization of magnetic MOFs

The magnetic composites of Fe_3O_4@PAA@MOF-199s were obtained by a two-step self-assembly approach. The crystalline structures and phase composition of Fe_3O_4@PAA submicrospheres and Fe_3O_4@PAA@MOF-199 were characterized by PXRD. As shown in Fig. 1, six diffraction peaks in the pattern of Fe_3O_4@PAA at 2θ=30.2° (220), 35.7° (311), 43.4° (400), 53.7° (422), 57.4° (511), and 62.9° (440) can be indexed to a typical phase of Fe_3O_4, which are in good agreement with the characteristic peaks of standard magnetite crystal (JCPDS No. 19-0629, isometric-hexoctahedral crystal system). In addition, XPS was performed to analyze the chemical states of iron (Supporting information, Fig. S1). The peaks at about 710 eV and 720 eV, corresponding to Fe 2p3/2 and Fe 2p1/2, confirms that the obtained submicrospheres consist of pristine Fe_3O_4. FTIR spectrum of Fe_3O_4@PAA (Supporting information, Fig. S2) also demonstrated the formation of the composite, in which, the absorption band at about 1452 cm^{-1} correspond to the -CH_2- bending vibration of the PAA chain, the absorption at about 1715 cm^{-1} is indicative of the C=O stretching, and the absorption bands at about 1571 cm^{-1} and 1407 cm^{-1} are assigned to asymmetric and symmetric stretching of the COO^-, respectively. Based on the calculations with the Debye-Scherrer formula for the strongest (311) diffraction peak, the size of Fe_3O_4 nanocrystals was *ca*. 15 nm. Comparing with the PXRD pattern of pristine MOF-199, Fe_3O_4@PAA@MOF-199 (H) shows almost the same diffractions, indicating MOF-199 structure was well developed. Because of the limited amount of Fe_3O_4 in Fe_3O_4@PAA@MOF-199 (H), as well as the overlap of diffractions of Fe_3O_4 and MOF-199 somehow, the diffractions of Fe_3O_4 is not clearly observed. Moreover, the FTIR spectra of Fe_3O_4@PAA, MOF-199, and Fe_3O_4@PAA@MOF-199 (Supporting information, Fig. S2) further demonstrates the successful formation of Fe_3O_4@PAA@MOF-199 composites.

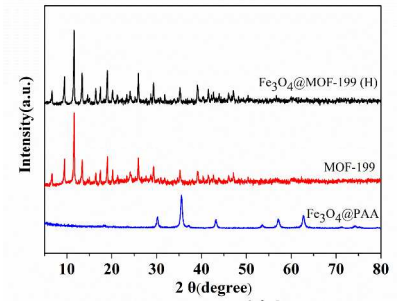

Fig. 1 X-ray diffraction patterns of Fe_3O_4@PAA, MOF-199 and Fe_3O_4@PAA@MOF-199 (H).

Fig. 2 shows the morphology of the magnetic particles. The FESEM images of Fe_3O_4@PAA (Fig. 2a) reveal that the submicrospheres obtained by the solvothermal method are uniform, with an average size of about 600 nm. Each Fe_3O_4@PAA microsphere consists of small Fe_3O_4 nanocrystals, which are enwrapped by PAA chains, and finally aggregated to large submicrospheres due to the tendency of reducing the strong surface tension. The SEM image of Fe_3O_4@PAA@MOF-199 (Fig. 2b) shows that Fe_3O_4@PAA submicrospheres are embedded in the continuous framework of MOF-199 crystals. Whereas its TEM image (Fig. 2c and 2d) further reveals that MOF-199 crystals grow up at the surface of Fe_3O_4@PAA submicrospheres and these submicrospheres are distributed in the MOF-199 matrix. Fig. 3 shows the bright-field TEM image of Fe_3O_4@PAA@MOF-199 and its corresponding EDS elemental mapping of Cu, C, Fe, O respectively. With denser Cu and C closely surrounded the core of Fe_3O_4, it confirms that Fe_3O_4@PAA submicrospheres are indeed embedded in MOF-199 crystals. Whereas O mapping image indicates that it distributes all over the materials with relatively denser in the core due to the contributions of both Fe_3O_4 and PAA. More importantly, no matter the elemental mapping of C or of O, both distributions are evenly without any voids between Fe_3O_4@PAA core and MOF-199 shell, indicating MOF-199 crystals are closely packed around the surface of Fe_3O_4@PAA submicrospheres, and further confirm the formation mechanism as proposed in scheme 1, that carboxyl groups in PAA chain can coordinate with Cu^{2+} cations to form the first seed layer of MOF-199, and induce the further growth of MOF-199 crystals around the core of Fe_3O_4@PAA. To illustrate the important role of PAA in the formation of the composite, we dispersed Fe_3O_4 nanoparticles and Fe_3O_4@PAA submicrospheres into $Cu(NO_3)_2$ solution, respectively. The ICP-AES results, as listed in Table S1, reveal that there is almost no copper ion absorbed in Fe_3O_4, whereas the content of copper ions in Fe_3O_4@PAA is as high as 80 mg/g, suggesting the carboxyl group in PAA chain can strongly coordinate with copper ions. The closely attached copper ions could form the first seed layer of MOF-199 at the surface of Fe_3O_4@PAA submicrospheres and hence further growth of MOF-199 crystals can be achieved. This following growth of MOF-199 was analogized to the Fe_3O_4@PAA@MOF-199 submicrospheres (Supporting information, Fig. S3) obtained by

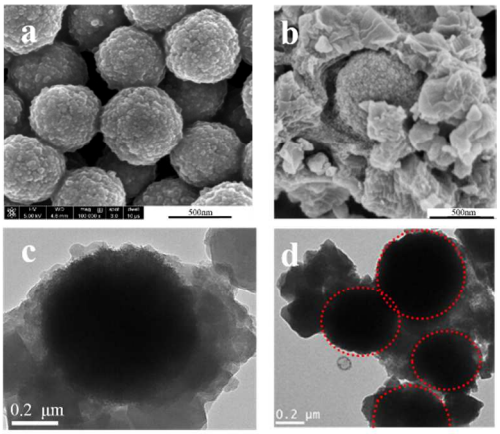

Fig. 2 SEM images of Fe_3O_4@PAA (a), Fe_3O_4@PAA@MOF-199 (b) and TEM images of Fe_3O_4@PAA@MOF-199 (c, d).

the complex LBL method, which can further illustrate the reality of our formation mechanism. However, in some of these work, Fe_3O_4@PAA submicrospheres are not totally coated by MOF-199 crystals due to the orientated growth of MOF crystals in one-pot synthesis. But we achieved significantly improved synthesis conditions, including the solvent changes from the expensive and hazardous DMF to the common solvent of ethanol, and the reaction time is greatly shortened to 2 h compared with the normal reaction time of 20 h[30] to meet with great favour for the future industrial applications. In fact, just because of these growth defects, some parts of the magnetite Fe_3O_4@PAA were exposed, which would present a stronger magnetism for the magnetic separation.

The amount of MOF-199 existed in the composite of Fe_3O_4@PAA@MOF-199 was determined by TGA. Fig. 4a shows the TGA curves of Fe_3O_4@PAA@MOF-199 (H), Fe_3O_4@PAA@MOF-199 (L) and pristine MOF-199. For the TGA curve of pristine MOF-199, there is a significant mass loss between 343 ^oC to 369 ^oC, ascribed to the decomposition of the structure. The mass lose was calculated as about 24.2 % in this temperature interval. Taking pristine MOF-199 as a reference, the mass lose of Fe_3O_4@PAA@MOF-199 (L) and Fe_3O_4@PAA@MOF-199 (H) in the same temperature interval was determined as about 22.9 % and 18.7 %, accordingly, the amount of MOF-199 in Fe_3O_4@PAA@MOF-199 (L) and Fe_3O_4@PAA@MOF-199 (H) were calibrated to be 93.4 % and 77.3 %, respectively, by a corresponding proportional relationship. The specific surface area and porous structures of the Fe_3O_4@PAA@MOF-199s were characterized by nitrogen adsorption at 77 K. As shown in Fig. 4b, the isotherms of Fe_3O_4@PAA@MOF-199 (H) and Fe_3O_4@PAA@MOF-199 (L) are a typical type I isotherms, which is the characteristic of microporous MOF-199. The hysteresis loops in high pressure range indicate the existence of macropores, attributed to the packing of MOF-199 particles and some voids between Fe_3O_4@PAA submicrospheres and MOF-199 particles. The specific surface area of the samples was calculated to be

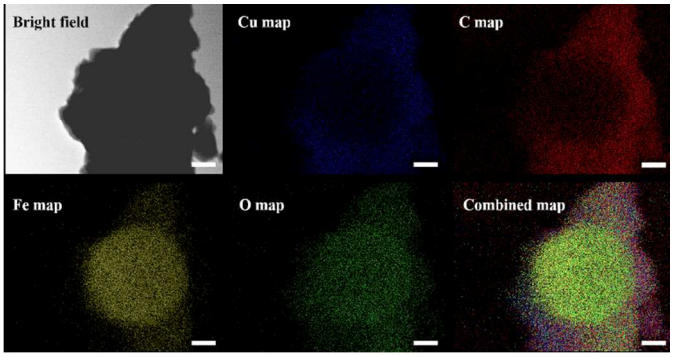

Fig. 3 Bright field transmission electron micrograph, Cu, C, Fe, O and combined elemental mapping images of Fe_3O_4@PAA@MOF-199, scale bar: 200 nm

824 m^2/g and 863 m^2/g for Fe_3O_4@PAA@MOF-199 (H) and Fe_3O_4@PAA@MOF-199 (L), respectively (Supporting information, Table S2). Compared with the specific surface area of pristine MOF-199 of 1286 m^2/g, the decrease of the specific surface area is mainly caused by the incorporation of Fe_3O_4@PAA, consequently, the lower quantities of MOF-199 in Fe_3O_4@PAA@MOF-199 (H), the relatively lower surface area.

Desulfurization performance

To decide an appropriate adsorption time, the adsorption profiles of DBT, BT and thiophene in model oil (5 mL) on Fe_3O_4@PAA@MOF-199 (H) (0.02 g) at 25 °C were conducted. As shown in Fig. 5, the adsorption quantity of S-compounds on Fe_3O_4@PAA@MOF-199 (H) initially increases rapidly. After that, the adsorption capacity reaches a saturated plateau and almost remains unchanged even with prolonging the adsorption time. For DBT, BT and thiophene, the saturated time is about 2.5 h, 1.5 h and 1 h, respectively, suggesting the larger the S-compound molecule, the longer the saturated adsorption. Thus, 3 h was selected as an appropriate adsorption time in the following study. Fig. 6 shows the adsorption isotherms of DBT, BT and thiophene in the model oil on Fe_3O_4@PAA@MOF-199 (H) and Fe_3O_4@PAA@MOF-199 (L) and their corresponding Langmuir plots at 25 °C. The adsorption quantity of Fe_3O_4@PAA@MOF-199s increase with increasing equilibrium concentration; and Fe_3O_4@PAA@MOF-199 (L) shows higher

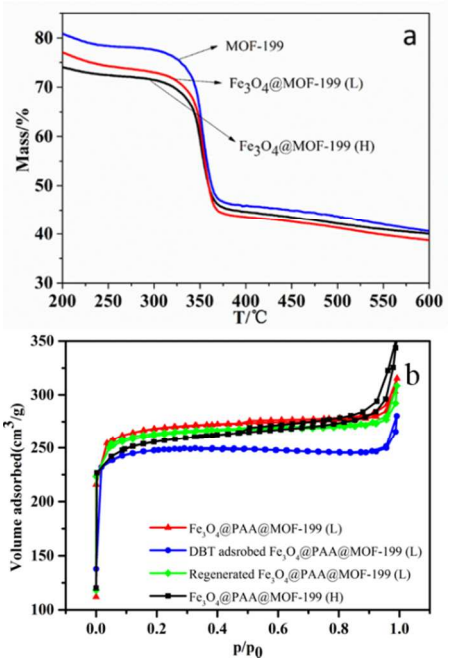

Fig. 4 (a) TGA curves (b) Nitrogen adsorption-desorption isotherms of Fe_3O_4@PAA@MOF-199s before and after the desulfurization.

adsorption capacity than Fe_3O_4@PAA@MOF-199 (H). The saturated adsorption capacity can be estimated by using the plotting of C_e/q against C_e, as shown in Fig. 6, the linear straight lines suggest the experimental results perfectly match with the Langmuir model. As summarized in Table 1, the values of the saturation adsorption capacity and the Langmuir constant of both Fe_3O_4@PAA@MOF-199s follow the order of DBT > BT > thiophene, which is in agreement with the electron density distribution on the S-compounds, revealing the adsorption capacity is mainly ascribed to the interaction between S-atom and metal ions in MOFs through π-complexation.[29] The saturated adsorption capacities on Fe_3O_4@PAA@MOF-199 (H) are calculated as 35.0, 15.9 and 11.8 mg S•g^{-1} for DBT, BT and thiophene, respectively.

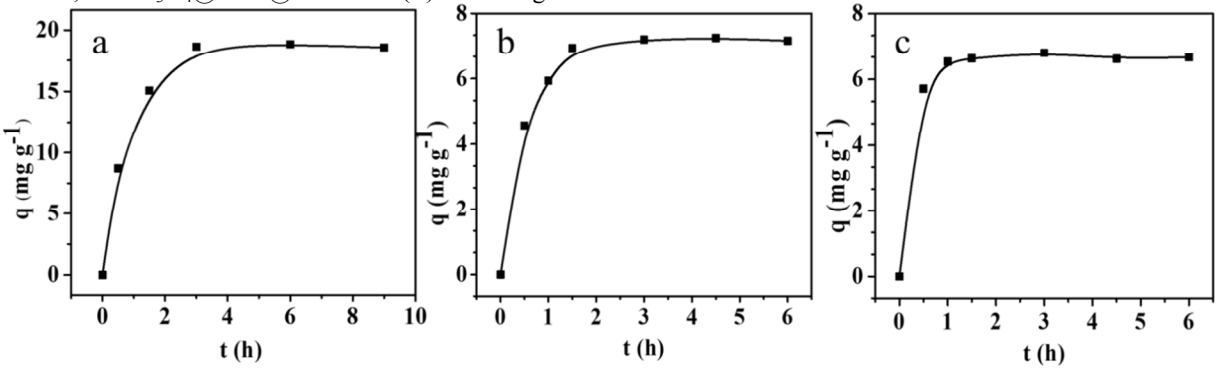

Fig. 5 Adsorption profiles of (a) DBT (C_0=371 mg/L), (b) BT (C_0= 401 mg/L) and (c) thiophene (C_0= 463 mg/L) in n-Octane on Fe_3O_4@PAA@MOF-199 (H) at 25 °C.

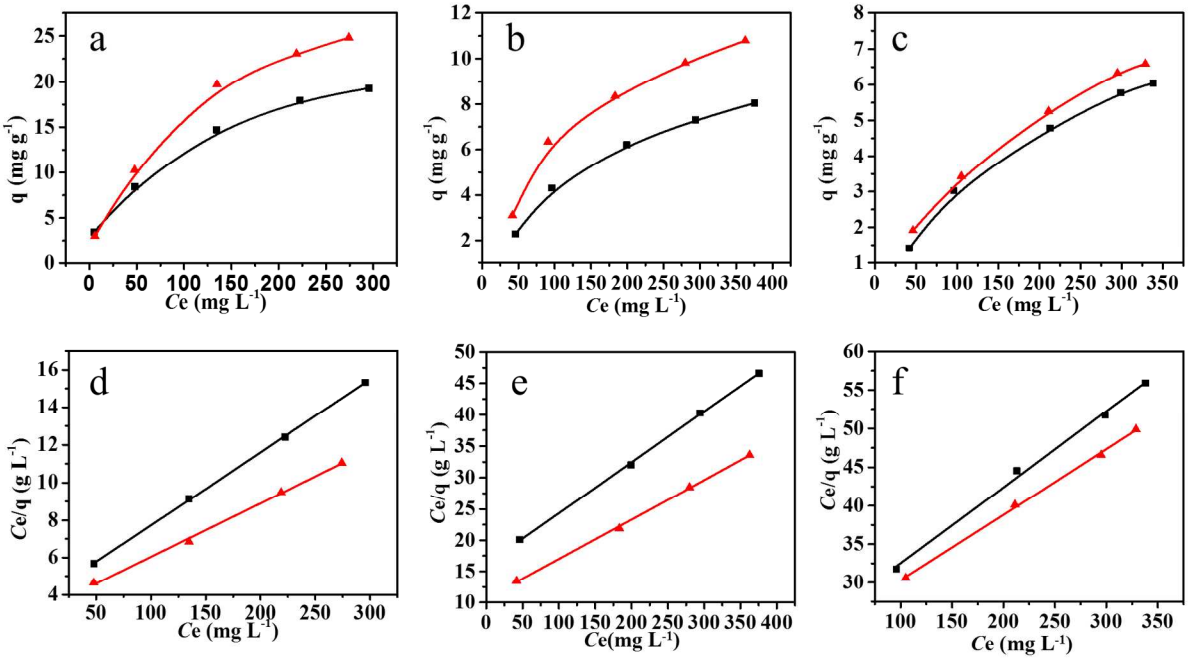

Fig. 6 Adsorption isotherms of (a) DBT, (b) BT, (c) thiophene and their corresponding Langmuir model plots of (d) DBT, (e) BT, (f) thiophene on Fe_3O_4@PAA@MOF-199 (H) (■) and Fe_3O_4@PAA@MOF-199 (L) (▲) after equilibrium for 3 h at 25 °C.

Table 1 Adsorption parameters of Fe_3O_4@PAA@MOF-199s based on Langmuir model [a]

Adsorbents	S-compound	Q_0(mg•g^{-1})	b (L•mg^{-1})	R	Q_{MOF}(mg•g^{-1}MOF)[b]
Fe_3O_4@PAA @MOF-199(L)	DBT	35.0	0.00899	0.99686	37.0
	BT	15.9	0.00588	0.99897	17.0
	thiophene	11.8	0.00389	0.99814	12.6
Fe_3O_4@PAA @MOF-199(H)	DBT	25.8	0.0101	0.99967	33.4
	BT	12.4	0.00496	0.99936	16.0
	thiophene	10.1	0.00437	0.99518	13.1
MOF-199	DBT				45[c]
MOF-199	BT				25[c]

[a]Q_0 and b are saturated adsorption capacity and Langmuir constant (L•mg^{-1}), respectively. [b]Q_{MOF} adsorption capacity, calibrated into per gram of MOF-199, [c]Adsorption capacity of pristine MOF-199 is collected from the literature.[15]

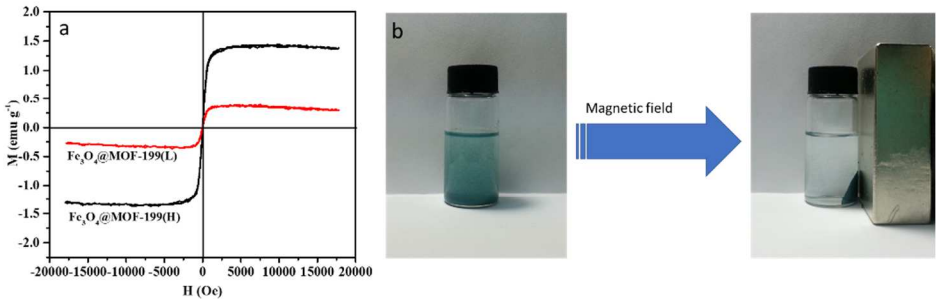

Fig. 7 (a) Magnetization as a function of magnetic field for Fe_3O_4@PAA@MOF-199 (H) and Fe_3O_4@PAA@MOF-199 (L) at 25 °C. (b) Photographs of Fe_3O_4@PAA@MOF-199 (H) in n-Octane before and after the magnetic separation.

Table 2 Saturation magnetization and turbidity of Fe_3O_4@PAA@MOF-199s

Adsorbents	M (emu•g^{-1})[a]	Turbidity (NTD)	DBT Adsorption capacity (mg•g^{-1})
Fe_3O_4@PAA@MOF-199(L)	0.3	6.8	37.0
Fe_3O_4@PAA@MOF-199(H)	1.4	2.1	33.4
MOF-199		92.0	

[a]M represents saturated mass magnetization obtained from VSM.

Moreover, according to the MOF quantities in Fe_3O_4@PAA@MOF-199s determined by TGA, the adsorption capacity of S-compounds of per gram MOF-199 on the obtained adsorbents were calibrated and compared with that on the pristine MOF-199. Take the adsorption capacity of DBT on Fe_3O_4@PAA@MOF-199 (H) for example, it is estimated to be 37.0 mg S• (g MOF)$^{-1}$, which is quite coincided with the reported data[15]. In addition, due to the higher quantities of MOF-199 in Fe_3O_4@PAA@MOF-199 (L), the adsorption capacity in Fe_3O_4@PAA@MOF-199 (L) is higher than Fe_3O_4@PAA@MOF-199 (H).

Recyclability and regeneration performance

Magnetization is the most important parameter for the effective magnetic separation. Fig. 7a shows the hysteresis loop of typical magnetic MOFs measured by sweeping the external magnetic field between -1.75 and +1.75 T at the room temperature. No obvious remanence or coercivity is observed in the magnetization curve, suggesting the soft magnetic character. The saturated mass magnetization of Fe_3O_4@PAA@MOF-199 (L) and Fe_3O_4@PAA@MOF-199 (H) are estimated to be 0.3 emu•g^{-1} and 1.4 emu•g^{-1}, respectively. Although the values of the saturated mass magnetization of Fe_3O_4@PAA@MOF-199s are not high, the magnetic separation can still be successfully applied for separating Fe_3O_4@PAA@MOF-199s from the oil (Fig. 7b). The separation performance was determined by measuring the turbidity of the oil. As shown in Table 2, the turbidity of the oil after magnetic separation for Fe_3O_4@PAA@MOF-199 (L) and Fe_3O_4@PAA@MOF-199 (H) is 6.8 NTD and 2.1 NTD, respectively. Comparing with the pristine MOF-199, after the magnetic separation, its turbidity value is as high as 92.0 NTD due to no magnetic property in pristine MOF-199, suggesting the magnetic separation for Fe_3O_4@PAA@MOF-199s is significantly effective. Combining the desulfurization and magnetic separation properties, Fe_3O_4@PAA@MOF-199 (H) shows better performance than Fe_3O_4@PAA@MOF-199 (L). Therefore, incorporating suitable amount of magnetite Fe_3O_4@PAA submicrospheres, which insures the magnetic separation efficiency without reducing the adsorption capacity, is a key point for successfully fabricating the magnetic adsorbent Fe_3O_4@PAA@MOF-199.

In the real application, the adsorbents should be renewable to reduce the operation cost. Therefore, the recycling stability is a crucial parameter. To investigate the regeneration performance, we selected p-xylene as the elution solvent to regenerate the Fe_3O_4@PAA@MOF-199. After a cycle of desulfurization, magnetic separation and regeneration by the solvent of p-xylene, the similar XRD patterns of Fe_3O_4@PAA@MOF-199 (H) before and after the desulfurization (Supporting information, Fig. S4) indicate the good stability of Fe_3O_4@PAA@MOF-199. Moreover, the TEM images of Fe_3O_4@PAA@MOF-199 (Fig. S5) show the adsorbent still kept its original morphology that Fe_3O_4@PAA submicrospheres were stably embedded in MOF-199 matrix. Accordingly, we can infer that Fe_3O_4@PAA submicrospheres have strong interaction with MOF-199 crystals, which can only be ascribed to the coordination interaction between carboxyl groups in PAA chains and copper cations in MOF-199 crystals. Besides, the nitrogen adsorption-desorption isotherms of Fe_3O_4@PAA@MOF-199 (L) before and after the desulfurization of DBT was compared in Fig. 4b and the textural properties of the samples before and after the desulfurization are summarized in Table S2 as well. Both the specific surface area and total pore volume slightly decreased after a cycle of desulfurization and regeneration. The specific surface area of Fe_3O_4@PAA@MOF-199 (L) decreased from 863 to 792 m^2/g after the saturation adsorption of DBT. However, after regeneration by p-xylene, the specific surface area can recover to 844 m^2/g. The effect of the regeneration times on the adsorption capacity is shown in Fig. 8. We can see that Fe_3O_4@PAA@MOF-199 (H) shows quite good adsorption stability for at least five times recycle. In comparison with the fresh adsorbent, the adsorption capacity decreases only by less than 9 % until the fifth regeneration. Therefore, the adsorbent of Fe_3O_4@PAA@MOF-199 can be easily regenerated after the desulfurization and exhibits a relatively stable recyclability.

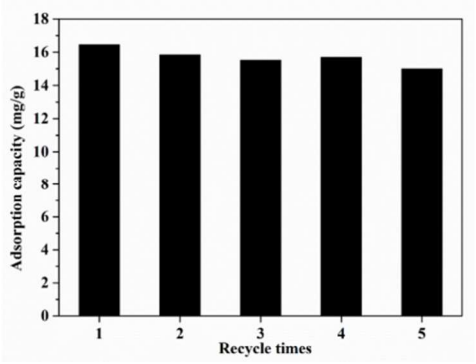

Fig. 8 Regeneration performance of Fe_3O_4@PAA@MOF-199 (H) for desulfurization of DBT in n-Octane at 25 °C (C_e=130 mg/L).

Conclusions

A new type magnetic adsorbent of Fe_3O_4@PAA@MOF-199 was prepared using a two-step assembly approach, in which PAA acted like a bridge to connect the magnetic Fe_3O_4 nanocrystals and MOF-199 crystals together. The Fe_3O_4@PAA@MOF-199 adsorbent showed quite good adsorption capacity for various thiophenic compounds in the model fuel, and followed the order of DBT > BT > thiophene due to the electron density distribution on the S-atom in these S-compounds. Meanwhile, the magnetic Fe_3O_4@PAA@MOF-199 adsorbent was beneficial in the utilization of magnetic separation. Moreover, the Fe_3O_4@PAA@MOF-199 adsorbent exhibited stable recyclability. We expect that this novel idea of designing and fabricating magnetic MOFs could provide potential method for the adsorptive desulfurization, as well as the magnetic separation.

Acknowledgements

This work is supported by the National Basic Research Program of China (2013CB733501), the National Natural Science Foundation of China (Nos. 21176066, 21376074), the program of FP7-PEOPLE-2013-IRSES (PIRSES-GA-2013-612230), the 111 Project of Ministry of Education of China (No. B08021) and the Fundamental Research Funds for the Central Universities of China.

Notes and references

[a]State Key Laboratory of Chemical Engineering and Department of Chemistry, East China University of Science and Technology, Shanghai, 200237, China
Tel & Fax: +86-21-64252195. Email: junhu@ecust.edu.cn.
Tel & Fax: +86-21-64252328. Email: linghao@ecust.edu.cn.
[b]Shanghai Institute of Measurement and Testing Technology, 1500 Zhangheng Road, Shanghai 201203, China

Electronic Supplementary Information (ESI) available: Supporting XPS measurement of Fe_3O_4@PAA, FTIR spectra of products, SEM images of Fe_3O_4@PAA@MOF-199 through 'LBL' method, X-ray diffraction pattern of fresh and regenerated Fe_3O_4@PAA@MOF-199 (H), TEM images of Fe_3O_4@PAA@MOF-199 after the desulfurization, copper (II) content in Fe_3O_4 and Fe_3O_4@PAA and textural parameters of Fe_3O_4@PAA@MOF-199s. See DOI: 10.1039/b000000x/

1 V. L. Nevel, I.Verbist, C. Harper, S. Byners, P. Smeyers, Y. Aregbe, P. Robouch, P. Taylor, G. Turk, R. Vocke and W. Kelly, IMEP report for European CommissionEUR21765EN. http://irmm.jrc.ec.europa.eu/html/interlaboratory_comparisons/imep/imep-18/EUR21765EN.pdf.
2 Z. Varga and J. Hancsok, *Petroleum & Coal*,2003, **45**, 135.
3 R. T. Yang, A. J. Hernández-Maldonado and F. H. Yang, *Science*,2003, **301**, 79.
4 Z. C. Li, H. P. Li, H. Zhao and G. Q. Wu, *Contemporary Chemical Industry*, 2013, **11**, 1588.
5 V.C. Srivastava, *RSC Adv.*,2012, **2**, 759.6 J. Xiao, X. X. Wang, M. Fujii, Q. J. Yang and C. S. Song, *AIChE J.*,2013, **59**, 1441.
7 A. Takahashi, R. T. Yang, C. L. Munson and D. Chinn, *Langmuir*, 2001, **17**, 8405.
8 A. J. Hernández-Maldonado, F. H. Yang, G. Qi and R. T. Yang, *Appl. Catal., B*,2005, **56**, 111.
9 K. Tang, X. Hong, Y. H. Zhao and Y. G. Wang, *Pet. Sci. Technol.*,2011, **29**, 779.
10 Y. Wang and R. T. Yang, *Langmuir*,2007, **23**, 3825.
11 H.-J. Jeon, C. H. Ko, S. H. Kim and J.-N. Kim, *Energy Fuels*,2009, **23**, 2537.
12 L. Wang, R. T. Yang and C.-L. Sun, *AIChE J.*,2013, **59**, 29.
13 R. T. Yang, A. Takahashi and F. H. Yang, *Ind. Eng. Chem. Res.*,2001, **40**, 6236.
14 S. Velu, X. L. Ma and C. S. Song, *Ind. Eng. Chem. Res.*,2003, **42**, 5293.
15 K. A. Cychosz, A. G. Wong-Foy and A. J. Matzger, *J. Am. Chem. Soc.*,2008, **130**, 6938.
16 K. A. Cychosz, A. G. Wong-Foy and A. J. Matzger, *J. Am. Chem. Soc.*,2009, **131**, 14538.
17 H. X. Zhang, H. L. Huang, C. X. Li, H. Meng, Y. Z. Lu, C. L. Zhong, D. H. Liu and Q. Y. Yang, *Ind. Eng. Chem. Res.*,2012, **51**, 12449.
18 N. A. Khan and S. H. Jhung, *Angew. Chem. Int. Ed.*,2012, **51**, 1198.
19 S. S.-Y. Chui, S. M.-F. Lo, J. P. H. Charmant, A. G. Orpen and I. D. Williams, *Science*,1999, **283**, 1148.
20 H. Gu, K. Xu, C. Xu and B. Xu, *Chem. Commun.*,2006, 941.
21 M. Lewin, N. Carlesso, C.-H. Tung, X.-W. Tang, D. Cory, D. T. Scadden and R. Weissleder, *Nat. Biotechnol.*, 2000, **18**, 410.
22 S. Miltenyi, W. Müller, W. Weichel and A. Radbruch, *Cytometry*,1990, **11**, 231.
23 J. H. Park, G. V. Maltzahn, E. Ruoslahti, S. N. Bhatia and M. J. Sailor, *Angew. Chem. Int. Ed.*,2008, **120**, 7394.
24 L. S. Zhong, J. S. Hu, H. P. Liang, A. M. Cao, W. G. Song and L. J. Wan, *Adv. Mater.*,2006, **18**, 2426.
25 E. Maxwell and D. Kelland, *IEEE T MAGN.*,1978, **14**, 482.
26 F. Ke, L. G. Qiu, Y. P. Yuan, X. Jiang and J. F. Zhu, *J. Mater. Chem.*,2012, **22**, 9497.
27 M. R. Lohe, K. Gedrich, T. Freudenberg, E. Kockrick, T. Dellmann, S. Kaskel, *Chem. Commun.*,2011, **47**, 3075.
28 J. Liang, H. Ma, W. Luo and S. Wang, *Mater. Chem. Phys.*,2013, **139**, 383.
29 C. Yu, X. M. Fan, L. M. Yu, T. J. Bandosz, Z. B. Zhao, J. S. Qiu, *Energy Fuels.*,2013, **27**, 1499.
30 A. R. Millward and O. M. Yaghi, *J. Am. Chem. Soc.*,2005, **127**, 17998.

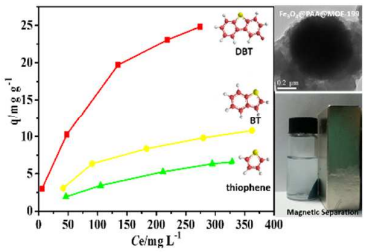

Novel magnetic Fe_3O_4@PAA@MOF-199 adsorbents showed a good desulfurization capacity, high magnetic separation efficiency, as well as a stable recyclability.